Article

Journal of Industrial Textiles

2016, Vol. 45(6) 1504–1515

DOI: 10.1177/1528083714564633
jit.sagepub.com
SAGE

Thermal and mechanical behavior of innovative melt-blown fabrics based on polyamide nanocomposites

Andrea Dorigato[1], Marco Brugnara[2], Gianmarco Giacomelli[3], Luca Fambri[1] and Alessandro Pegoretti[1]

Abstract

A commercial organo-modified clay (OMC) was added to a polyamide 6 (PA6) matrix at various concentrations during the polymerization stage or by melt compounding in a twin-screw extruder, and the resulting pellets were used for the production of depth filters in the shape of cylindrical nonwoven webs through a melt-blown process. The processability of the investigated materials was significantly affected by nanofiller introduction. Differential scanning calorimetry revealed that OMCs play a nucleating effect on the crystallization of the polyamide matrix, with a remarkable increase in the crystallization temperature on cooling from the melt. Consequently, a parameter related to the filtering performances of the web, such as the pressure drop (ΔP) evaluated on cylindrical filters, decreased with the increase in die-to-collector distance in a more pronounced way for nanocomposite nonwovens. This behavior was related to the significant decrease of the connecting points in the networks due to the rapid cooling of the filaments on the collecting mandrel. Compressive mechanical tests evidenced how organoclay addition led to a remarkable increase of the rigidity of the web, when the data were compared at the same ΔP value, irrespectively from the preparation technique.

Keywords

Organo-modified clay, polyamide 6, filtration, meltblowing, nanocomposites

[1]Department of Industrial Engineering, University of Trento, Trento, Italy
[2]UFI Innovation Center Srl, Corso Trento 20, Ala, Italy
[3]Aquafil Spa, Via Linfano 9, Arco, Italy

Corresponding author:
Andrea Dorigato, Department of Industrial Engineering, University of Trento, Via Mesiano 77, Trento 38123, Italy.
Email: andrea.dorigato@ing.unitn.it

Introduction

Nowadays, nonwoven fabrics manufactured from polymeric fibers are extensively applied for air and liquid filtration in the automotive field and industrial equipments due to their low cost and high efficiency [1]. Because of their good properties such as high porosity, large surface area, dust-free, low-cost, and easy processability, these fabrics can also be suitable for hygienic and medical use [2]. Nonwovens can be manufactured through various technologies such as wet- or dry-laid, spun-bond or melt-blown, and are in general composed of fine fibers assembled together to form a web. Depending on the selected process, fibers are either bonded with adhesives or binders, thermally through calendering or, in particular, in the melt-blown process, physically linked due to the connection between partially solidified fibers forming a self-bonded nonwoven web.

Because of their good drawability and their similarity to silk fibers, aliphatic polyamides (nylons) were initially applied in various textile applications (garments, carpets, rugs, etc.) [3]. Nowadays, polyamides (PAs) are widely utilized in fiber, film, packaging, and molding applications [4]. PA6 is one of the most widely used polyamides. Every year, about 4.3 million tons of caprolactam are produced worldwide to synthesize PA6 for massive application, also including nonwoven fabrics for the automotive field.

In the last two decades it has been widely proven how the mechanical performance (such as elastic modulus, fracture toughness, and tensile properties at break) of several polymeric matrices could be significantly improved through the addition of quite limited amounts (generally less than 5 wt%) of nanostructured materials [5]. In particular, substantial improvements of the thermomechanical properties of polymer matrices were obtained through the addition of high aspect ratio fillers, such as carbon nanotubes [6] and clays [7]. From an industrial point of view, layered silicates (montmorillonites) are among the most investigated nanofillers [8,9]. These nanofillers are characterized by a lamellar structure, consisting of two-dimensional layers about 1 nm thick and 200–300 nm long, where a central octahedral sheet of alumina or magnesia is alternated with two external silica tetrahedrons. These layers are stacked with a regular van der Waals gap between them. Negative charges generated by isomorphic substitution within the layers are generally counterbalanced by Na^+ or Ca^{2+} cations located in the interlayer galleries. Considering that the forces that hold the stacks together are relatively weak, the intercalation of small molecules between the layers can be easily performed [10]. In order to obtain a more organophilic clay, the hydrated cations of the interlayer can be exchanged with cationic surfactants such as alkylammonium or alkylphosphonium salts [11,12], thus obtaining an organo-modified clay (OMC). The thermomechanical behavior of polymer-clay nanocomposites is strictly connected to the dispersion level of the clay in the polymer matrix, which in turn is determined by the filler–matrix interactions [13]. When the polymer is unable to intercalate between the silicate sheets, a phase separated microcomposite is formed. Intercalated structure can be obtained when polymer chains are present in the

interlayer galleries of the silicate, resulting in a well ordered multilayer morphology built up with alternating polymeric and inorganic layers. When the silicate layers are completely and uniformly dispersed in a continuous polymer matrix, an exfoliated (or delaminated) structure is obtained [14]. Despite the large amount of experimental results on PA6/organoclay nanocomposites, less attention was devoted to the investigation of the thermomechanical behavior of PA6 nanocomposite melt-blown fabrics.

Starting from the above considerations, the aim of the present work is to perform a detailed thermomechanical characterization of PA6 nanocomposite melt-blown fabrics prepared by dispersing various amounts of a commercial OMC by using two different processing techniques (*in situ* polymerization and melt compounding). The role of the most important manufacturing parameters on the microstructural, thermal, and mechanical behaviors of the resulting materials was highlighted.

Experimental section

Various amounts (from 1 to 5 wt%) of OMC were dispersed in a commercial PA6 (AQ), provided by Aquafil s.p.a Arco (Trento, Italy), in two different ways: (i) during the polymerization of the PA6 matrix (*in situ* polymerization, P) or (ii) by melt compounding (C) in a twin-screw extruder.

Samples were denoted indicating the matrix (AQ), the technique adopted for filler dispersion (C or P) and the nanofiller weight fraction. For instance, AQ-P-3 indicates the nanocomposite sample filled with 3 wt% of OMC dispersed during the polymerization stage.

The resulting materials have been then pelletized and utilized for the production by a melt-blown process of cylindrical depth filters, having a height of 80 mm, an inner diameter of 30 mm and a mean wall thickness of about 5 mm. Samples were prepared by varying die-to-collector distance (DCD) in the range from 120 to 300 mm, keeping the same melt pressure into the die, same polymer, and air throughput. In order to reach a constant moisture content, samples were stored at 23°C and at a relative humidity of 50% up to a constant weight was reached (generally within 15 days). In Figure 1(a) and (b), representative images of the cylindrical filters utilized in this work are reported.

By considering that the fiber diameter was the same for all samples, as well as the deposited mass, different DCD induced different amount of fiber cross links and so a different filter structure. The filter structure was correlated to the measured pressure drop under a given air flow. In other words, the pressure drop (ΔP) of the samples gave an indirect indication of the morphology of the nonwoven fabric in terms of physical links in the network. The pressure drop was measured by blowing compressed air through the filter. The flow direction was from inside to outside. The flow was regulated by a needle valve and the flow was measured with a Comhas VA420 flowmeter. The ΔP value was measured through a Delta Ohm HD2164.2 manometer. A representative picture of the pressure drop measurement

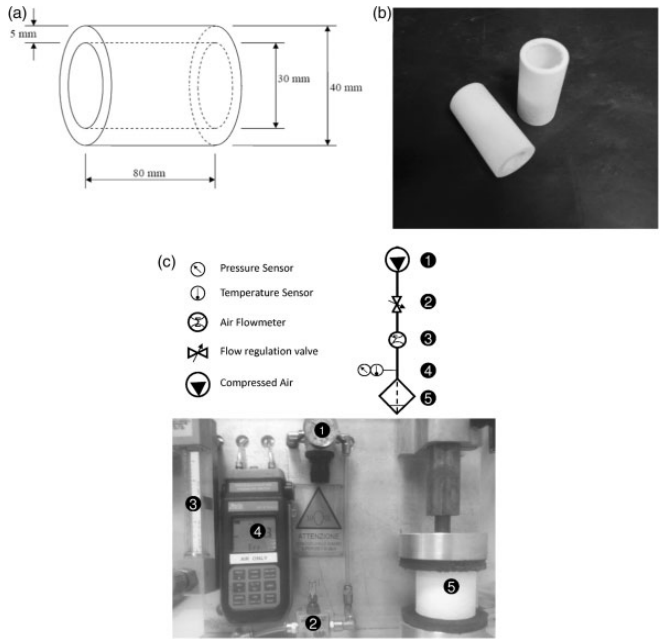

Figure 1. Representative images of the cylindrical filters used in this work: (a) geometry of the samples, (b) picture of AQ-P-1 filters. (c) representative picture of the pressure drop measurement apparatus.

apparatus is reported in Figure 1(c). Therefore, considering that depth filters are made with the same amount of polymer mass, we can consider that two filters have the same structure when they show the same air pressure drop.

Field emission scanning electron microscope (FESEM) observations of the filters were performed through a Zeiss Supra 40 microscope, operating at a voltage of 30–50 kV. In order to reach the highest magnifications, single fibers were extracted from the filters and embedded in a conductive paste. After the solidification of the paste, samples were cryofractured in liquid nitrogen and observed.

Thermal properties of the materials were evaluated through differential scanning calorimetry (DSC) by a Mettler Toledo DSC30 apparatus under a nitrogen flow of 100 mL/min. After a first heating run from 0°C to 270°C at 10°C/min, a cooling step down to 0°C and a second heating run at the same rate were performed. The second heating run was performed to evaluate the thermal properties of the tested materials after making their thermal histories uniform by melting and cooling under controlled conditions. The glass transition temperature (T_g) values were determined from the inflection point of DSC thermograms at around 50°C, while the melting temperature (T_m) was measured in correspondence to the melting peak. As indicated in equation (1), the crystallinity degree was evaluated

normalizing the specific energy of the melting peak (ΔH_m) by the standard enthalpy of the fully crystalline PA6 (ΔH_0), taken as 190 J/g [15]

$$\chi = \frac{\Delta H_m}{\Delta H_0} \tag{1}$$

Mechanical characterization of the cylindrical filters was performed through an Instron 4502 tensile testing machine. Cylindrical filters were compressed perpendicularly to their axis at a crosshead speed of 50 mm/min, testing at least five specimens for each sample. A rigidity value (K) was determined from the initial slope of the force-displacement curves (avoiding the first 0.5 mm part in which a nonperfect linear behavior was displayed), and the force at 10 mm displacement ($F_{10\text{mm}}$) was calculated.

Results and discussion

Microstructural analysis

It is well known that the mechanical behavior of nonwovens is strongly influenced by the morphological features of the resulting web. Therefore, microstructural analysis can provide a significant contribution to investigate the interconnection state of the web and the nanofiller dispersion within the matrix. In Figure 2(a) to (c), the microstructural features of AQ-P-1 sample are represented. Figure 2(a) highlights how the nonwovens are characterized by a dense web of randomly oriented PA6 fibers with diameters lower than 10 μm. From that micrograph, no physical bonds between filaments can be detected. This probably means that fiber solidification occurred before they reached the collection mandrel. From the FESEM image of a single filament at 30,000× magnifications reported in Figure 2(b), some circular cavities on the fracture surface can be detected. The presence of the OMC can be better evaluated in Figure 2(c), in which nanofiller appears to be homogeneously distributed in the polymer matrix, forming aggregates of stacked lamellae about 200 nm long and with a mean thickness lower than 30 nm. Therefore, it can be concluded that the adopted process parameters lead to a quite homogeneous nanofiller dispersion within the polymer matrix.

Thermal properties

In Figure 3(a) to (c), DSC thermograms of neat AQ and of the relative nanocomposite chips collected during the heating and the cooling stages are reported, while in Figure 3(d) the trends of the crystallization temperature as a function of the OMC content are reported. Moreover, in Table 1 the main parameters detected from DSC tests are summarized. Double melting peaks displayed by nanofilled

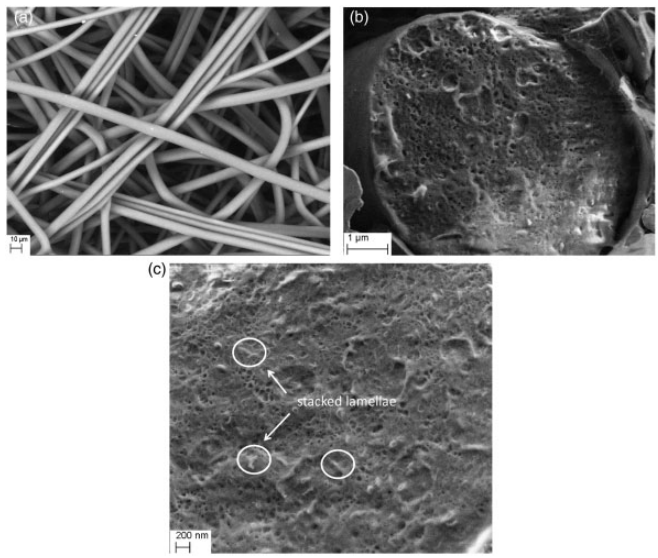

Figure 2. Microstructural features of AQ-P-1 samples. (a) FESEM micrograph of the web, (b) FESEM image of the cryofractured section of a single fiber at 30,000× and (c) 50,000× magnifications.

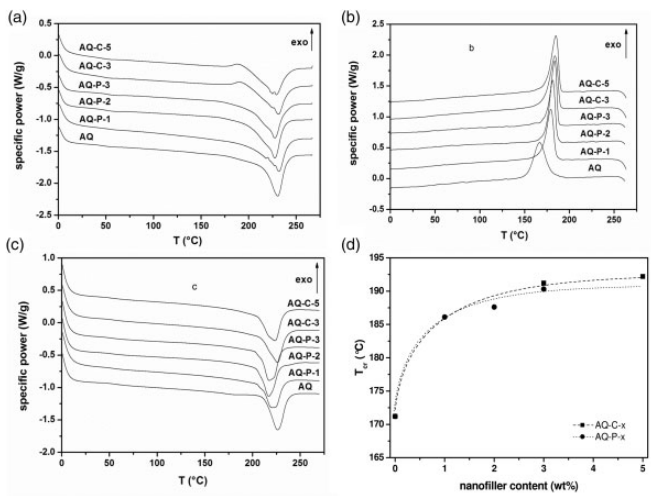

Figure 3. DSC tests on neat AQ and relative nanocomposite chips. Representative thermograms collected during (a) the first heating stage, (b) the cooling stage and (c) the second heating stage. (d) crystallization temperature of (■) AQ-C-*x* and (●) AQ-P-*x* samples (*x* = 1 – 5 wt%).

Table 1. Results of DSC tests on neat AQ and the corresponding nanocomposite chips.

Sample	T_{g1} (°C)	T_{m1} (°C)	X_1 (%)	T_c (°C)	X_c (%)	T_{g2} (°C)	T_{m2} (°C)	X_2 (%)
AQ	47.4	226.3	49.5	171.2	34.4	56.6	222.1	34.4
AQ-P-1	49.3	226.6	45.0	186.1	30.8	52.0	215.5	31.4
AQ-P-2	48.8	223.1	48.2	187.6	30.3	50.2	213.5	33.5
AQ-P-3	50.0	223.2	48.3	190.3	32.6	51.5	212.6	33.8
AQ-C-3	45.1	226.4	35.2	191.2	36.1	52.7	220.8	36.4
AQ-C-5	44.4	224.2	36.5	192.2	35.0	50.9	218.4	38.2

Tg1: glass transition temperature during the first heating stage; Tm1: melting temperature during the first heating stage; X1: crystallinity degree during the first heating stage; Tc: crystallization temperature during the cooling stage; Xc: crystallinity degree during the cooling stage; Tg2: glass transition temperature during the second heating stage; Tm2: melting temperature during the second heating stage; X2: crystallinity degree during the second heating stage.

samples in Figure 3(a) are due to the presence of two different crystalline fractions induced by the different thermal histories of the materials during the production process. In fact, in the second heating run (Figure 3(b)) the thermal history of the materials is homogenized, and only a single peak can be detected. While the melting point of the samples (T_{m1} and T_{m2}) is unaffected by the presence of the nanofiller, a remarkable shift of the crystallization peak (T_c) towards higher temperatures can be noticed in the cooling scan, regardless of the dispersion mode. For instance, a T_c increase of about 20°C with respect to the neat AQ matrix can be observed with a OMC content of about 3 wt%. This means that OMC plays a distinct nucleating effect on the polymer chains. Moreover, the data reported in Figure 3(d) clearly indicate presence of quite similar effects independent of the dispersion method adopted for nanocomposites preparation (either *in situ* polymerization or melt compounding). The nucleating effect of OMCs on the crystallization of PA6 has been widely documented in the scientific literatures [16–18].

Mechanical behavior

In order to better understand the influence of the processing parameters on the morphology of the resulting cylindrical filters, air pressure drop (ΔP) values under standard conditions were correlated to the DCD values both for neat and nanocomposite nonwovens (Figure 4). As expected, ΔP decreases by increasing the DCD values, because the solidification of the filaments before the winding stage leads to a noticeable decrease of the connecting points in the networks and to a less connected structure. Interestingly, this aspect is even more pronounced in the nanofilled samples, in which the crystallization of the molten polymer is faster, being promoted by the presence of organoclay (see DSC tests).

Therefore, the mechanical properties of the investigated webs were strongly dependent on the thermal properties of the materials and on the processing

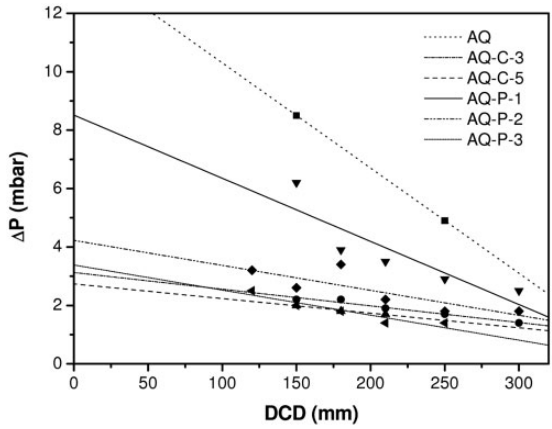

Figure 4. Pressure drop (ΔP) as a function of the die-to-collector distance (DCD) of neat AQ and relative nanocomposite filters, with the respective linear fitting lines. (■) AQ, (▼) AQ-P-1, (♦) AQ-P-2, (◄) AQ-P-3, (●) AQ-C-3, (▲) AQ-C-5.

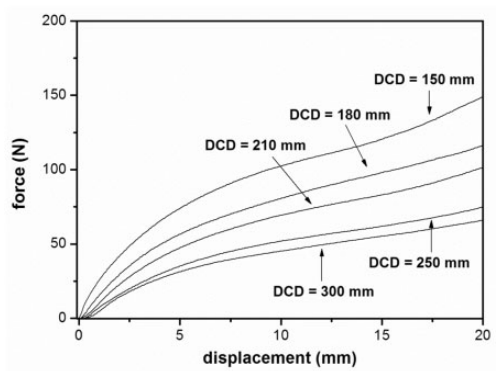

Figure 5. Representative force–displacements curves from compressive tests on neat AQ filters prepared at different DCD values.
DCD: die-to-collector distance.

conditions. In order to confirm this hypothesis, quasi-static compressive tests were performed. In Figure 5, representative force–displacement curves from compression tests on neat AQ filters prepared at different DCD values are represented, while in Figure 6(a) and (b) the stiffness (K) and the force at 10 mm displacement ($F_{10\text{mm}}$) values are respectively reported. It can be noticed how the mechanical properties of the prepared cylinders (both K and $F_{10\text{mm}}$) decrease with the DCD values, because of the decrease of the number of junctions in the nonwoven web. This trend is even more pronounced when nanocomposites at elevated filler

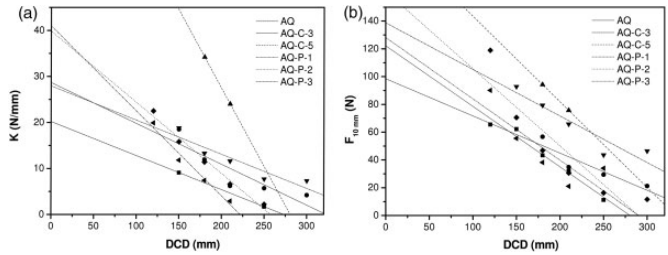

Figure 6. (a) stiffness and (b) force at 10 mm displacement (F_{10mm} from compressive tests on neat AQ and relative nanocomposite filters, with the respective linear fitting lines. (■) AQ, (▼) AQ-P-1, (♦) AQ-P-2, (◄) AQ-P-3, (●) AQ-C-3, (▲) AQ-C-5.
DCD: die-to-collector distance.

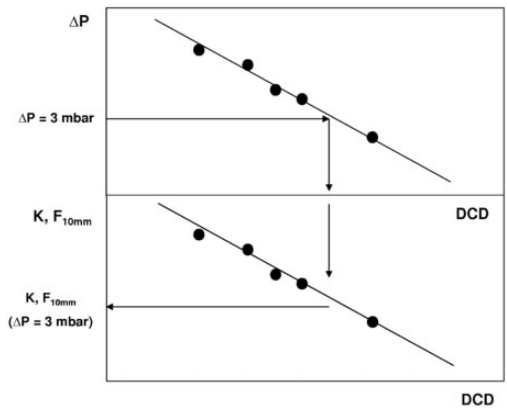

Figure 7. Representation of the experimental procedure to correlate the pressure drop to the corresponding compressive properties of the cylindrical filters.
DCD: die-to-collector distance.

amounts are considered. Once again, the nucleating effect of the nanofiller promoted a rapid solidification of the filaments, thus reducing the interconnection points of the webs over the whole range of investigated DCD values.

In order to highlight the contribution of the nanofiller addition on the mechanical properties of the prepared filters, it is necessary to compare the mechanical properties of the cylindrical filters at the same ΔP values (i.e. at the same number of network junctions and fibers density). In Figure 7, a schematic representation of the experimental procedure to correlate the pressure drop to the corresponding compressive properties of the cylindrical filters is reported. For each formulation, it is possible to identify a DCD value corresponding to a ΔP of 3 mbar (taken as a reference value, the corresponding air flow is 2500 L/min). It is therefore possible to detect the K and F_{10mm} values associated with this DCD value.

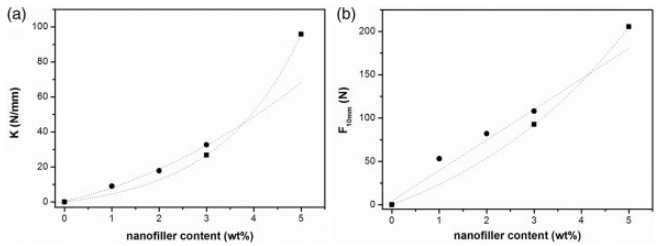

Figure 8. Stiffness (K) and force at 10 mm displacement (F_{10mm}) at a pressure drop of 3 mbar of neat AQ and relative nanocomposite filters. (■) AQ-C-x and (●) AQ-P-x samples (x = 1 – 5 wt%).

Therefore, stiffness (K) and force at 10 mm displacement (F_{10mm}) values at the same pressure drop (of 3 mbar) can be reported in Figure 8(a) and (b) for neat AQ and relative nanocomposite filters. It can be concluded that, if the same pressure drop (i.e. the same web structure of the nonwoven web) is considered, the introduction of organoclay leads to a noticeable improvement of the mechanical properties, especially at elevated filler amount. From these results, it is difficult to assess the real influence of the OMC dispersion technique on the compressive performances of the filters. However, it is clearly demonstrated how nanofiller introduction strongly affects both the processing parameters and the morphology of the filters, improving the intrinsic mechanical performances of PA6 nonwoven filters.

Therefore, a proper selection of DCD values for the nanofilled samples leads to the production of nanocomposite filters with strongly improved compressive properties. It is also interesting to observe that the data reported in Figure 8(a) and (b) indicate a quite similar behavior for nanocomposites prepared by *in situ* polymerization (P) or by melt compounding (C). This last experimental evidence is clearly related to the crystallization behavior of the nanocomposites quantified by thermal calorimetry.

Conclusions

Various amounts (from 1 to 5 wt%) of an OMC have been dispersed in a commercial PA6 matrix directly during the polymerization stage or by melt compounding in a twin-screw extruder, and the resulting compounds were then utilized for the preparation of innovative melt-blown fabrics to be then thermomechanically characterized.

DSC tests revealed that nanoclay addition plays a nucleating effect on the PA6 matrix, with a shift of the crystallization peak towards higher temperatures and then on the processing condition in the production of a nonwoven. Therefore, to compare the increase of mechanical properties due to nanofiller addition, filters with a similar microstructure should be compared. This could be performed by considering filters showing the same pressure drop, i.e. a technological parameter determined by the filter microstructure. The variation of the pressure drop with the

DCD values was more pronounced for nanocomposite nonwovens, because the effect of nanofillers as nucleating agents led to a faster crystallization of the filaments and thus to a noticeable decrease of the connecting points in the networks.

Also, the mechanical properties of the prepared materials were strongly affected by their microstructural features and it was concluded that, if the same pressure drop value was considered, nanoclays introduction led to a noticeable rigidity increase, irrespective of the preparation technique.

Declaration of Conflicting Interests

The author(s) declared no potential conflicts of interest with respect to the research, authorship, and/or publication of this article.

Funding

The author(s) disclosed receipt of the following financial support for the research, authorship, and/or publication of this article: This research activity has been supported by the Provincia Autonoma di Trento (PAT) through the project Better Resistance Across Clays's Evolutions (BRACE).

References

[1] Teodorescu HN, Dascalescu L, Hulea M, et al. Correlations between the electric charging properties and the optically determined structure of non-woven fabrics. *J Electrostat* 2013; 71: 635–647.
[2] Hou X, Zhang T and Cao A. A heparin modified polypropylene non-woven fabric membrane adsorbent for selective removal of low density lipoprotein fromplasma. *Polym Adv Technol* 2013; 24: 660–667.
[3] Hsiao S, Wang H, Chou J, et al. Synthesis and characterization of novel organosoluble and thermally stable polyamides bearing triptycene in their backbones. *J Polym Res* 2012; 19: 9902–9911.
[4] Kohan MI. *Nylon plastics handbook*. Munich: Hanser, 1995.
[5] Hussain F. Polymer-matrix nanocomposites, processing, manufacturing, and application: An overview. *J Compos Mater* 2006; 40: 1511–1575.
[6] Huang YY and Terentjev EM. Dispersion of carbon nanotubes: Mixing, sonication, stabilization, and composite properties. *Polymers* 2012; 4: 275–295.
[7] Chiu CW, Huang TK, Wang YC, et al. Intercalation strategies in clay/polymer hybrids. *Prog Polym Sci* 2014; 39: 443–485.
[8] Alexandre M and Dubois P. Polymer-layered silicate nanocomposites: Preparation, properties and uses of a new class of materials. *Mater Sci Eng R: Rep* 2000; 28: 1–63.
[9] Giannelis EP, Krishnamoorti R and Manias E. Polymer-silica nanocomposites: Model systems for confined polymers and polymer brushes. *Adv Polym Sci* 1999; 118: 108–147.
[10] Theng BKG. *The chemistry of clay-organic reactions*. London: Adam Hilger Ltd, 1974.
[11] Kovarova L, Kalendova A, Gerard J, et al. Structure analysis of PVC nanocomposites. *Macromol Symp* 2005; 221: 105–114.
[12] Peprnicek T, Kalendova A, Pavlova E, et al. Polyvinylchloride-paste/clay nanocomposites : Investigation of thermal and morphological characteristics. *Polym Degrad Stab* 2006; 91: 3322–3329.

[13] Pegoretti A, Dorigato A and Penati A. Contact angle measurements as a tool to investigate the filer-matrix interactions in polyurethane-clay nanocomposites from blocked prepolymer. *Eur Polym J* 2008; 44: 1662–1672.
[14] Song, Hu Y, Tang Y, et al. Study on the properties of flame retardant polyurethane/organoclay nanocomposite. *Polym Degrad Stab* 2005; 87: 111–116.
[15] Kaisersberger E, Knappe S and Mohler H. Thermal analyses for polymer engineering; dsc,tg, dma. In: *Netzsch annual for science and industry*. Vol. 2Selb-Wurzburg, Germany, 1993.
[16] Bureau MN, Denault J, Cole KC, et al. The role of crystallinity and reinforcement in the mechanical behavior of polyamide-6/clay nanocomposites. *Polym Eng Sci* 2002; 42: 1897–1906.
[17] Fornes TD and Paul DR. Crystallization behavior of nylon 6 nanocomposites. *Polymer* 2003; 44: 3945–3961.
[18] Lincoln DM, Vaia RA, Wang ZG, et al. Temperature dependence of polymer crystalline morphology in nylon 6/montmorillonite nanocomposites. *Polymer* 2001; 42: 9975–9985.